

SUBMILLIMETER H₂O MEGAMASERS IN NGC 4945 AND THE CIRCINUS GALAXY

D. W. PESCE

Department of Astronomy, University of Virginia, 530 McCormick Road, Charlottesville, VA 22904, USA

J. A. BRAATZ

National Radio Astronomy Observatory, 520 Edgemont Road, Charlottesville, VA 22903, USA

C. M. V. IMPELLIZZERI

National Radio Astronomy Observatory, 520 Edgemont Road, Charlottesville, VA 22903, USA
 and

Joint Alma Office, Alonso de Cordova 3107, Vitacura, Santiago, Chile

ABSTRACT

We present 321 GHz observations of five AGN from ALMA Cycle 0 archival data: NGC 5793, NGC 1068, NGC 1386, NGC 4945, and the Circinus galaxy. Submillimeter maser emission is detected for the first time towards NGC 4945, and we present a new analysis of the submillimeter maser system in Circinus. None of the other three galaxies show maser emission, though we have detected and imaged the continuum from every galaxy. Both NGC 4945 and Circinus are known to host strong ($\gtrsim 10$ Jy) 22 GHz megamaser emission, and VLBI observations have shown that the masers reside in the innermost ~ 1 parsec of the galaxies. The peak flux densities of the 321 GHz masers in both systems are substantially weaker (by a factor of ~ 100) than what is observed at 22 GHz, though the corresponding isotropic luminosities are more closely matched (within a factor of ~ 10) between the two transitions. We compare the structure of the submillimeter spectra presented here to the known 22 GHz spectra, and we argue that in both galaxies the 321 GHz emission likely originates from the same material that gives rise to the 22 GHz masers. The continuum emission in NGC 4945 and NGC 5793 shows a spatial distribution indicative of an origin in the galactic disks (likely thermal dust emission), while for the other three galaxies the emission is centrally concentrated and likely originates from the nucleus.

Keywords: masers — galaxies: active — galaxies: nuclei

1. INTRODUCTION

Nuclear water vapor megamasers currently provide the only direct means to map gas in active galactic nuclei (AGN) on size scales of ~ 0.1 – 1 pc. Nearly all of the observational work on H₂O megamasers to date has focused on the $6_{16} - 5_{23}$ rotational transition at 22.235 GHz from the ortho-H₂O molecule (Lo 2005). More than 160 galaxies have been detected in this line so far, the result of some ~ 4000 galaxies surveyed (e.g., Braatz et al. 2015). About 130 of the detections are associated with AGN, where they are called megamasers because of their large apparent luminosities. The physical con-

ditions that give rise to maser activity at 22 GHz are also compatible with masing in other transitions of the H₂O molecule, many of which fall in the submillimeter wavelength band (Neufeld & Melnick 1991; Gray et al. 2016).

Humphreys et al. (2005) presented the first observations of H₂O megamaser emission in a transition other than the 22 GHz, detecting maser emission at 183 GHz and (tentatively) at 439 GHz towards the galaxy NGC 3079. This galaxy had previously been known to host strong 22 GHz masers (Henkel et al. 1984), with VLBI observations confirming that the 22 GHz emission originates from the galactic nucleus (Trotter et al. 1998). Though the signal-to-noise of the (sub)millimeter detections ($\sim 7\sigma$ for the 183 GHz transition) was too low

to permit detailed study, the maser emission appears to arise from several narrow (spectrally unresolved) features spanning a velocity range comparable to that of the 22 GHz emission.

The 183 GHz transition was also detected towards Arp 220 by [Cernicharo et al. \(2006\)](#), where it displays a very broad ($\sim 350 \text{ km s}^{-1}$) and almost featureless spectral line structure. Interestingly, this galaxy has not been detected in 22 GHz emission (e.g., [Henkel et al. 1986](#)), suggesting that the masing gas has a low density ($n_{\text{H}_2} \lesssim 10^6 \text{ cm}^{-3}$) and temperature ($T \lesssim 100 \text{ K}$). From consideration of these physical conditions and the observed line width, [Cernicharo et al. \(2006\)](#) interpret the 183 GHz masers in this galaxy as likely originating from a large number ($\sim 10^6$) of dense molecular cores rather than being associated with the galactic nuclei.

More recently, [Hagiwara et al. \(2013\)](#) used ALMA to detect 321 GHz H_2O megamaser emission towards the Circinus galaxy, another strong 22 GHz nuclear megamaser host (e.g., [Greenhill et al. 2003b](#)). The sensitivity of the Circinus observation was sufficient to showcase the richness of the high-frequency maser spectrum, opening up for the first time the possibility of using submillimeter masers in ways that had heretofore been restricted to the 22 GHz transition.

In this paper we report the first detection of submillimeter maser emission from NGC 4945, and we present a new calibration of the maser spectrum for the Circinus galaxy. The observations and data reduction procedures are described in §2, and in §3 we discuss the submillimeter emission and compare the 321 GHz masers to those at 22 GHz. Throughout this paper we quote velocities using the optical definition in the heliocentric reference frame.

2. OBSERVATIONS AND DATA REDUCTION

We have analyzed archival Cycle 0 ALMA observations of five galaxies that are known to have strong (peak $S_\nu \gtrsim 200 \text{ mJy}$) 22 GHz water maser emission associated with a central AGN: NGC 1068 ([Claussen et al. 1984](#)), NGC 1386 ([Braatz et al. 1996](#)), NGC 4945 ([Dos Santos & Lepine 1979](#)), Circinus ([Gardner & Whiteoak 1982](#)), and NGC 5793 ([Hagiwara et al. 1997](#)). All targets were observed at a rest-frame frequency of 321.226 GHz (ALMA Band 7), which corresponds to the $10_{2,9} - 9_{3,6}$ rotational transition of ortho- H_2O ¹. NGC 5793 was further observed at a rest-frame frequency of 325.153 GHz, corresponding to the $5_{1,5} - 4_{2,2}$ rotational transition of para- H_2O . The total bandwidth for each dual-polarization observation was 1.875 GHz,

which was split into 3840 channels spaced contiguously every 0.488 MHz (corresponding to a velocity resolution of $\sim 0.5 \text{ km s}^{-1}$). The longest baselines for these observations were ~ 360 meters (corresponding to a typical resolution of $\sim 0.5''$), and there were between 18 and 25 antennas present (see Table 1).

We obtained datasets and initial calibration scripts from the ALMA archive; all post-processing reduction, imaging, and spectral analysis was done using the Common Astronomy Software Applications package (CASA)². Table 1 lists the observing parameters for each galaxy.

We detected and imaged continuum emission for all five sources (shown in Figure 1), and in NGC 4945 the continuum was strong enough for self-calibration. Two of the galaxies – Circinus and NGC 4945 – also host 321 GHz maser emission; we self-calibrated the Circinus data using the line emission.

2.1. Circinus

Initial imaging was performed using CASA task `clean` with natural UV weighting; after using `uvcontsub` (specifying line-free channels) to remove the continuum contribution, we separately imaged the line and continuum emission. We then performed several iterations of phase-only self-calibration, using the ~ 400 spectral channels with the strongest emission ($\gtrsim 100 \text{ mJy}$, corresponding to the velocity range $\sim 500\text{--}700 \text{ km s}^{-1}$) to determine the phase solutions. We found that a solution interval of 1 minute (averaging both polarizations) was optimal, yielding sufficiently continuous solutions (i.e., consecutive phase solution jumps of $\lesssim 30^\circ$) to confidently interpolate the phases. The calibration solutions were then applied to both the line and continuum data using `applycal`, and we stopped iterating self-calibration once there was no noticeable increase in signal-to-noise ratio (SNR). The resulting continuum image is shown in Figure 1, and the spectrum extracted from the (spatially unresolved) line-only data cube is shown in Figure 2.

2.2. NGC 4945

The maser emission in NGC 4945 is not sufficiently strong for self-calibration, so we used the continuum emission instead. Because the continuum emission in NGC 4945 is spatially resolved, we only used the longest baselines ($> 150 \text{ m}$, corresponding to the unresolved, point-like nuclear component of the emission) to determine the phase solutions that were then applied to the spectral line data; no such baseline restrictions were imposed when self-calibrating the continuum image it-

¹ Frequencies and quantum numbers have been taken from Splatalogue: <http://www.cv.nrao.edu/php/splat/>.

² <http://casa.nrao.edu/>

Table 1.

	NGC 5793		Circinus	NGC 4945	NGC 1068	NGC 1386
R.A. (J2000)	14:59:24.807		14:13:09.906	13:05:27.279	02:42:40.770	03:36:46.237
Dec. (J2000)	−16:41:36.55		−65:20:20.468	−49:28:04.44	−00:00:47.84	−35:59:57.39
v_{rec} (km s $^{-1}$)	3491		434	563	1137	868
Observing date (UTC)	2012 Jun 01	2012 Jun 03	2012 Jun 03	2012 Jun 03	2012 Jun 06	2012 Aug 24
ν_0 (GHz)	321.226	325.153	321.226	321.226	321.226	321.226
t_{int} (min.)	6.3	21.0	19.1	15.3	15.8	11.6
PWV (mm)	1.35	0.40	0.55	0.60	0.54	0.64
Antennas (number)	21	20	18	18	20	25
Flux calibrator	Titan	Titan	Titan	Titan	Uranus	Uranus
Bandpass calibrator	3C 279	3C 279	3C 279	3C 279	3C 454.3	3C 454.3
Phase reference	J1517–243	J1517–243	J1329–5608	J1325–430	J0339–017	J0403–36
Beam size (″)	0.55×0.47	0.66×0.46	0.66×0.50	0.56×0.52	0.66×0.45	0.96×0.53
Beam PA (°)	48	−89	−18	24	32	82
RMS $_s$ (mJy)	9.8	7.2	12.6 ^a	9.9	7.4	9.2
RMS $_c$ (mJy beam $^{-1}$)	0.39	0.29	0.48	3.0	0.42	0.36
R_{ap} (″)	2.5	2.5	2.0	5.0	1.5	1.0
S_ν (mJy)	10.8	18.8	90.8	733	47.1	4.3
σ_{S_ν} (mJy)	2.1	2.4	5.6	26.7	4.5	0.36 ^b
M_{ISM} (M_\odot)	4.0×10^8	6.6×10^8	...	1.5×10^8

NOTE—Information about the observations. Listed coordinates (rows “R.A.” and “Dec.” for right ascension and declination, respectively) correspond to the tracking center entered for the observations, which might not precisely match the location of the target (we note in particular that the tracking center for NGC 4945 is displaced by approximately 2.5 arcseconds from the position listed in NED). The “ v_{rec} ” row lists the galaxy recession velocity in km s $^{-1}$ (taken from NED), “ ν_0 ” gives the rest-frame observing frequency, “ t_{int} ” denotes the on-source integration time in minutes, and “PWV” is the average level of precipitable water vapor during the observation. Half-power beam widths (“beam size” row) for the imaged data are given in arcseconds, and the beam position angles (“beam PA” row) are measured in degrees east of north. The “RMS $_s$ ” row lists the typical spectral sensitivity reached per 2 km s $^{-1}$ vector-averaged channel, and the “RMS $_c$ ” row gives the brightness sensitivity of the continuum image. In general, the gradient in atmospheric opacity across a single spectrum causes the RMS $_s$ to increase by $\sim 30\%$ from one end to the other, so that the quoted value is an average. The bottom section of the table lists the gas masses calculated from continuum observations. R_{ap} gives the radius of the aperture used to measure the continuum flux density (centered on the peak of the continuum emission), S_ν is the flux density measured inside of that aperture, σ_{S_ν} is the uncertainty in flux density, and M_{ISM} is the ISM gas mass calculated using the method outlined in §3.1.

^aThe RMS $_s$ value for Circinus is given per 0.5 km s $^{-1}$ channel.

^bSince the continuum emission in NGC 1386 is unresolved, we measure the peak flux density instead of the integrated, and we use the RMS of the continuum image as the uncertainty in this value.

self. We used a solution interval of 30 seconds, averaging both polarizations. Despite repeated iterations of self-calibration, the sensitivity of the continuum image from this “snapshot” observation remains dynamic-range limited (see Vila Vilario et al. 2011). The resulting noise level of 3.0 mJy beam $^{-1}$ is thus larger than what one would nominally expect from a sensitivity calculation.

The rest of the reduction procedure matches what was done for Circinus (see §2.1). To account for the sizable ($\sim 2.5''$) offset of the emission center from the phase center, we used `impbcor` to apply a primary beam correction prior to extracting a spectrum from the data cube. The continuum image and spectrum for NGC 4945 are shown in Figures 1 and 3, respectively.

3. DISCUSSION

3.1. Continuum emission

The continuum structures for NGC 5793 and NGC 4945 are both elongated in one direction (spanning $\sim 4'' \approx 1000$ pc in NGC 5793, and $\sim 9'' \approx 160$ pc in NGC 4945), and both appear to have substantial substructure. Both of these galaxies are edge-on spirals, and the elongation axes of the submillimeter continua are aligned with the large-scale optical major axes (Gardner et al. 1992; Elmouttie et al. 1997). The continuum in NGC 4945 is also resolved along the minor axis, spanning $\sim 1.5'' \approx 30$ pc. All of this indicates that the continuum emission in these galaxies traces the galactic disks, rather than originating from, e.g., a molecular torus region around the central AGN (though there may be a contribution to the emission in the centermost regions from such material).

At these wavelengths ($\lambda \approx 940 \mu\text{m}$), the continuum in NGC 5793 and NGC 4945 is likely dominated by opti-

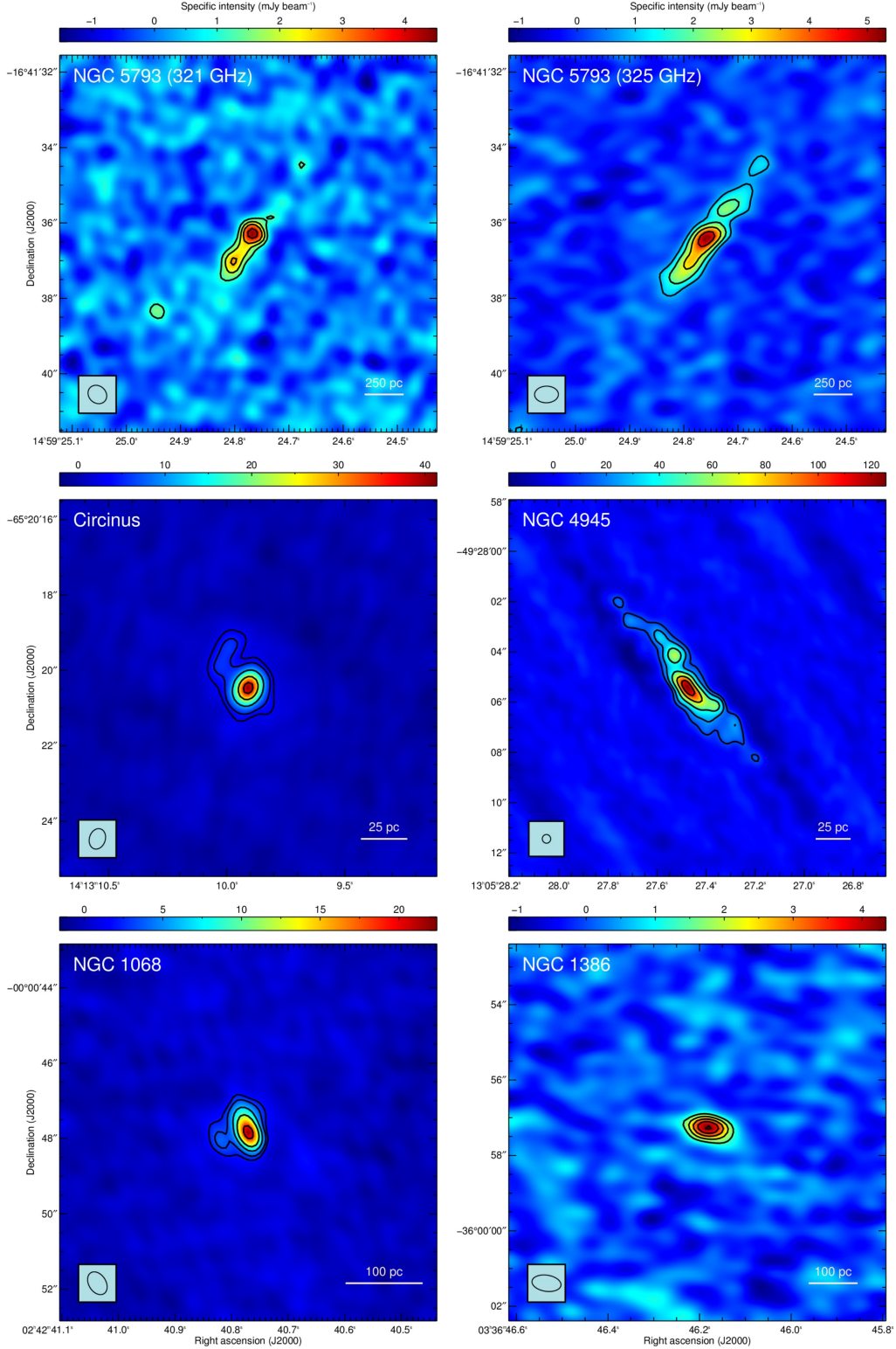


Figure 1. Continuum images. *Top left:* 321 GHz image of NGC 5793, with 3σ , 5σ , 7σ , and 10σ contours in black ($1\sigma = 0.39$ mJy beam $^{-1}$). *Top right:* 325 GHz image of NGC 5793, with 3σ , 6σ , 10σ , 15σ , and 20σ contours in black ($1\sigma = 0.29$ mJy beam $^{-1}$). *Center left:* 321 GHz image of Circinus, with 5σ , 10σ , 25σ , 50σ , and 75σ contours in black ($1\sigma = 0.48$ mJy beam $^{-1}$). *Center right:* 321 GHz image of NGC 4945, with 4σ , 8σ , 15σ , 25σ , and 35σ contours in black ($1\sigma = 3.0$ mJy beam $^{-1}$). *Bottom left:* 321 GHz image of NGC 1068, with 5σ , 8σ , 15σ , 25σ , and 45σ contours in black ($1\sigma = 0.42$ mJy beam $^{-1}$). *Bottom right:* 321 GHz image of NGC 1386, with 4σ , 6σ , 8σ , 10σ , and 12σ contours in black ($1\sigma = 0.36$ mJy beam $^{-1}$). Half-power restoring beam shapes are shown at the bottom left of each image, and scale bars are shown at the bottom right. For NGC 5793, we adopt a Hubble law distance of 50 Mpc, using $H_0 = 70$ km s $^{-1}$ Mpc $^{-1}$. We use distances of 10.1 Mpc for NGC 1068 and 15.9 Mpc for NGC 1386; these were measured by [Nasonova et al. \(2011\)](#) and [Tully et al. \(2013\)](#), respectively, using the Tully-Fisher relation.

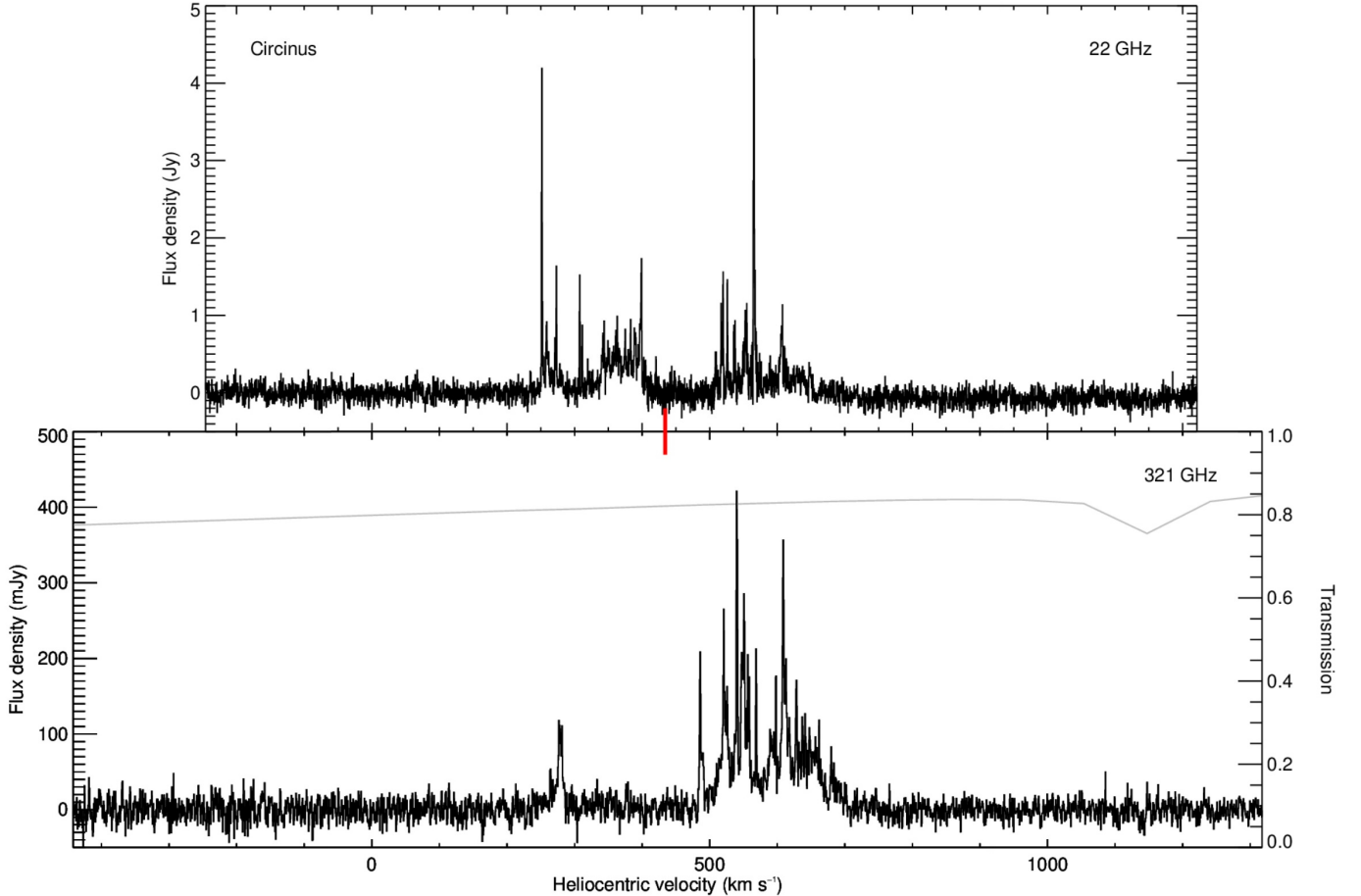


Figure 2. H₂O megamaser spectra of Circinus. *Top:* A reproduction of the 22 GHz spectrum taken with the 64 m Parkes telescope in 1998 August from Braatz et al. (2003). We have restricted the vertical axis range to more easily see the weaker features, resulting in the strongest feature (peaking at ~ 18 Jy) getting cut off. *Bottom:* 321 GHz spectrum extracted from the continuum-subtracted data cube. The channel width is 0.5 km s^{-1} . The atmospheric transmission curve, corresponding to a precipitable water vapor level matching that present during the observation, is overplotted in light grey. Atmospheric transmission curves have been taken from the Atacama Pathfinder Experiment (APEX) transmission calculator (<http://www.apex-telescope.org/sites/chajnantor/atmosphere/>). The recession velocity of the galaxy is marked by a vertical red line.

cally thin thermal (i.e. blackbody) emission from large dust grains (see, e.g., Draine 2003; Compiègne et al. 2011). The spectral energy distribution (SED) of such emission is typically modeled as a modified blackbody function (e.g., Planck Collaboration et al. 2014), with the free parameters being the optical depth τ , the dust temperature T_d , and the power-law index of the dust opacity β . With only a single SED point per galaxy, we must assume fiducial values for two of these parameters (e.g., β and T_d) to allow for a measurement of the third (e.g., τ). Further assumptions are then necessary to convert the optical depth to, e.g., a total interstellar medium (ISM) gas mass, M_{ISM} .

Fortunately, Scoville et al. (2014) have developed an empirical calibration of the relationship between dust emission and ISM gas mass. As long as the emission is measured in the Rayleigh-Jeans tail, the authors found that the calibration is relatively insensitive to whether

the ISM is dominated by atomic or molecular gas, if the galaxy is normal or undergoing a starburst, or whether the dust lies in the inner or outer regions of the galaxy. Rewritten in a suitable form, the conversion is given by

$$M_{\text{ISM}} = \frac{D^2 \lambda^2 S_\nu}{2k \kappa_{\text{ISM}} T_d}. \quad (1)$$

Here, D is the luminosity distance to the galaxy, λ is the observing wavelength, S_ν is the observed flux density, k is the Boltzmann constant, κ_{ISM} is the dust opacity per unit mass of ISM, and T_d is the dust temperature. Most of the underlying physics here is contained in κ_{ISM} , which the authors calibrated using *Planck* data to be

$$\left(\frac{\kappa_{\text{ISM}}}{4.84 \times 10^{-3} \text{ cm}^2 \text{ g}^{-1}} \right) = \left(\frac{\lambda}{850 \text{ } \mu\text{m}} \right)^{-\beta}. \quad (2)$$

When calculating gas masses, we use the results from Planck Collaboration et al. (2011) to fix $\beta = 1.8$, and

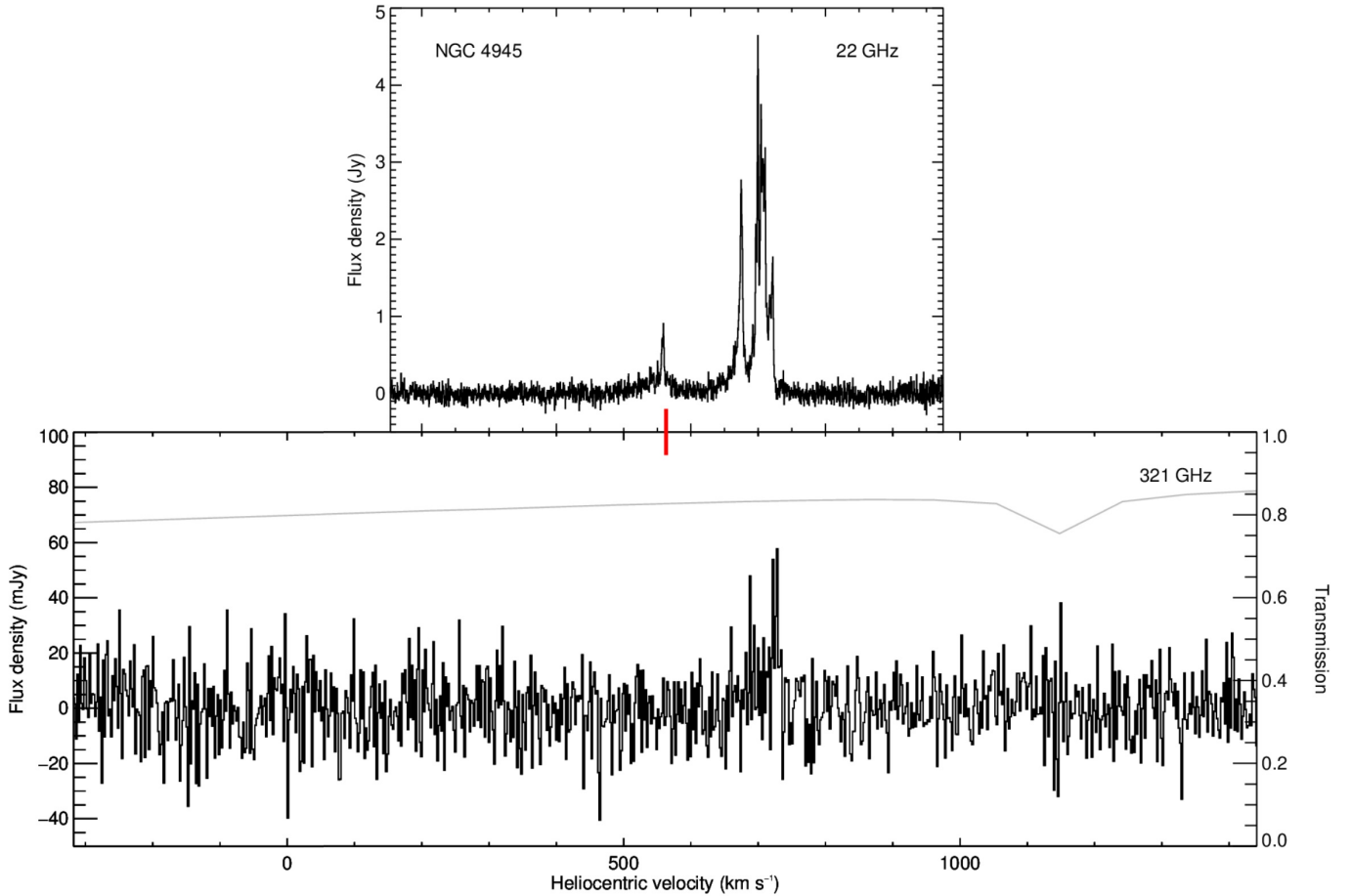


Figure 3. Same as Figure 2, but for NGC 4945. The channel size for the 321 GHz spectrum has been averaged to 2.0 km s^{-1} .

we adopt a dust temperature of $T_d = 25 \text{ K}$ (following [Scoville et al. 2014](#)). We measure the total continuum flux density for each galaxy using a circular aperture centered on the continuum peak, and we estimate the uncertainty using the dispersion of integrated flux densities measured in 15 non-overlapping, identical apertures that are offset from the continuum emission in the same image. The results from these measurements are presented in the bottom portion of Table 1. The gas masses estimated from the 321 GHz and 325 GHz observations of NGC 5793 are broadly consistent, while the estimate for NGC 4945 is somewhat lower.

NGC 1068, NGC 1386, and Circinus all show continuum emission considerably more centrally-concentrated than in NGC 5793 and NGC 4945, so it is likely that AGN contributions to the continua for these galaxies are not negligible. Disentangling the thermal (i.e., black-body) and nonthermal (e.g., electron-scattered synchrotron, free-free) components of the emission is non-trivial, and requires multi-frequency observations (see, e.g., [Krips et al. 2011](#)).

For NGC 1068, we can compare our observations to those of [García-Burillo et al. \(2014\)](#), who used ALMA to map the continuum at 349 GHz down to a 1σ level of

$0.14 \text{ mJy beam}^{-1}$. Though this is a factor of ~ 3 more sensitive than the map presented in this paper, we see consistent continuum structure and amplitude in the circumnuclear region (i.e., the region containing emission stronger than our sensitivity threshold) between the two observations.

3.2. 321 GHz H_2O masers in NGC 4945

The 321 GHz maser detection in NGC 4945 – which represents the first time such emission has been seen in this galaxy – is considerably fainter than in Circinus (Figure 3). Individual maser features are detected at the $\sim 4\text{--}5\sigma$ level, though the entire complex between 650 km s^{-1} and 750 km s^{-1} is detected at $\sim 9\sigma$ in integrated intensity. Adopting a distance to NGC 4945 of 3.7 Mpc ([Tully et al. 2013](#)), the observed flux of $0.88 \text{ Jy km s}^{-1}$ corresponds to an isotropic luminosity of $L_{\text{iso}} = 4 L_{\odot}$. Though the flux density of individual features is down by a factor of ~ 100 from what is observed at 22 GHz (e.g., [Braatz et al. 1996](#)), the isotropic luminosity is only lower by a factor of ~ 10 .

Insofar as we are able to discern spectral structure, we see that it appears to match reasonably well with previous observations of NGC 4945 at 22 GHz (top panel

of Figure 3 has been reproduced from Braatz et al. (2003). The increasing feature strength with increasing velocity and the overall appearance of 2–3 dominant features are both reminiscent of the 22 GHz spectra. However, the 321 GHz features at $\sim 687 \text{ km s}^{-1}$ and $\sim 726 \text{ km s}^{-1}$ (with possibly a third at $\sim 660 \text{ km s}^{-1}$) don’t map one-to-one with regions of 22 GHz emission. Rather, and quite intriguingly, the 321 GHz peaks fall precisely where the 22 GHz emission drops off.

Unlike with Circinus, the origin of the 22 GHz emission from NGC 4945 is not yet well understood. Greenhill et al. (1997b) made a VLBI map of NGC 4945 at 22 GHz using the southernmost antennas of the VLBA, and they found the spatial distribution of the masers to be approximately linear and distributed across $\sim 50 \text{ mas}$ ($\sim 0.9 \text{ pc}$) from one end to the other. This – in particular the roughly symmetric location of redshifted and blueshifted emission to either side of the systemic velocity – is suggestive of masers situated in an accretion disk. The limited antennas available for mapping such a low declination source (-49°) resulted in the map being rather incomplete (i.e., there were several systemic and blueshifted features that were too faint to map), but it is the best available for this source. We thus proceed with the disk interpretation.

Working under the assumption that the 321 GHz emission traces largely the same material as the 22 GHz, the observed 321 GHz features correspond only to the redshifted gas in the accretion disk. If the 321 GHz spectral structure follows that of the 22 GHz emission, then the undetected blue and systemic features would be slightly below our detection threshold.

3.3. 321 GHz H_2O masers in Circinus

Hagiwara et al. (2013) discovered the 321 GHz maser in Circinus. Here we re-examine the data, using strong maser lines to apply phase self-calibration (see §2.1). The new calibration improves the SNR by a factor of ~ 2 compared the initial analysis.

Published 22 GHz spectra of Circinus (e.g., top panel of Figure 2, reproduced from Braatz et al. 2003) show that the bulk of the maser emission occupies velocities between ~ 250 – 650 km s^{-1} more or less contiguously, though often with a notable paucity of features near the systemic velocity. Greenhill et al. (2003b) (hereafter G03) observed Circinus between 1997 and 1998 using the Australia Telescope Long Baseline Array. They detected two populations of masers, one arising from a warped accretion disk and the other associated with a wide-angle, bipolar outflow.

The 321 GHz masers are weaker in flux density by a factor of ~ 30 – 100 compared to their 22 GHz counterparts. Although the maser flux at 22 GHz is subject to interstellar scintillation (Greenhill et al. 1997a), this ef-

fect should be almost completely absent at 321 GHz (at such a high frequency, the diffractive scale of the turbulence will be much larger than the Fresnel scale; see Narayan 1992). At a distance to the galaxy of 4.2 Mpc (measured by Karachentsev et al. 2013 using the Tully-Fisher relation), the observed flux of $17.5 \text{ Jy km s}^{-1}$ corresponds to an isotropic luminosity of $\sim 104 L_\odot$; this is roughly a factor of four larger than the isotropic luminosity of the 22 GHz masers (e.g., Braatz et al. 1996).

The 321 GHz and 22 GHz spectra share broad structural similarities. Both have maser emission spanning comparable total velocity ranges and consolidated primarily into two groups located on either side of the systemic velocity, and in both cases the blueshifted group of features is weaker and sparser than the redshifted group. We can also see that the region around the systemic velocity in the 321 GHz spectrum is devoid of obvious features – either because no maser features exist at these velocities, or because they are below our detection threshold – which is reminiscent of the same segment of the 22 GHz spectrum.

The VLBI maps from G03 show that the extent of the 22 GHz maser emission in Circinus is roughly $50 \times 80 \text{ mas}$ ($\sim 1.0 \times 1.6 \text{ pc}$); assuming the 321 GHz maser spots are spatially distributed in approximately the same manner as the 22 GHz masers, this means that the distribution of the 321 GHz maser spots is spatially unresolved in the observations presented here (the beam size is $\sim 0.5''$). Though the absolute astrometric precision for ALMA observations is typically limited to ~ 0.05 arcseconds without taking special calibration steps (Remijan et al. 2015; Reid & Honma 2014), the relative uncertainty in point-source position within the same primary beam (as a fraction of the half-power beam width) is inversely proportional to the SNR (see, e.g., Fouque et al. 1990). Future high-resolution ALMA observations should thus have little difficulty mapping the 321 GHz masers in Circinus.

In lieu of a high angular resolution map, we can use the information contained in the spectrum to glean some understanding of the spatial distribution of the masers. By applying a threshold proximity of 1 mas between any individual maser spot and the disk midline, G03 were able to assign a rough classification to each maser as originating from either the disk or the outflow. In doing so, they found that the outflow masers dominated the emission between ~ 300 – 600 km s^{-1} , and that disk maser emission dominated blueward of $\sim 300 \text{ km s}^{-1}$ and redward of $\sim 600 \text{ km s}^{-1}$ (see Figure 6 in their paper). With this picture from G03 as a guideline, we can compare the spectral distribution of the 22 GHz masers to that of the 321 GHz masers.

Their similar overall spectral structure suggests that the 321 GHz and 22 GHz masers are tracing roughly

the same material. This is to be expected from consideration of the physical conditions required for strong maser activity in these transitions. Gray et al. (2016) have performed a thorough exploration of the relevant parameter space (i.e., gas density, kinetic temperature, and dust temperature) and found that the 321 GHz transition shares an optimal gas density ($n_{\text{H}_2} \approx 10^9 \text{ cm}^{-3}$) and collisional pumping scheme (i.e., low dust temperature) with the 22 GHz transition, though it prefers a somewhat larger kinetic temperature of $T_K \approx 1500 \text{ K}$ (compared to $T_K \approx 1000 \text{ K}$ for the 22 GHz transition). This could explain the apparent excess of 321 GHz maser emission between $\sim 650\text{--}750 \text{ km s}^{-1}$, which is not typically seen in 22 GHz spectra (though we note that 22 GHz emission has been seen out to velocities as large as $\sim 900 \text{ km s}^{-1}$, albeit with a much lower flux density than the bulk of the emission; see Greenhill et al. 2003a). Under this interpretation, the 321 GHz emission redward of 650 km s^{-1} originates in the accretion disk at radii interior to where 22 GHz emission is found.

We see no features in the 321 GHz spectrum between $\sim 300\text{--}500 \text{ km s}^{-1}$, which is a spectral range dominated by outflow emission at 22 GHz. Either the 321 GHz emission does not trace the outflow at all or the 321 GHz outflow masers in this velocity range are much fainter than their 22 GHz counterparts (i.e., down by a larger factor from the higher-velocity emission to either side). If the 321 GHz masers in fact only trace the disk emission, then the features detected between $\sim 500\text{--}600 \text{ km s}^{-1}$ indicate that some of these masers must originate farther out in the disk than the 22 GHz masers. Higher angular resolution observations will be able to discern whether any of the 321 GHz maser originate in the outflow or if they are all associated with the disk.

The possible high-velocity maser features – seen at $\sim 1070 \text{ km s}^{-1}$ and $\sim 1130 \text{ km s}^{-1}$ in the 321 GHz spectrum – coincide with an atmospheric absorption line (see Figure 2) and may represent elevated noise.

4. CONCLUSIONS

We present 321 GHz ALMA observations of NGC 5793, NGC 1068, NGC 1386, NGC 4945, and the Circinus galaxy. All galaxies are detected in continuum emis-

sion, and Circinus and NGC 4945 also display H_2O megamaser emission. For NGC 4945 these data represent the first detection of submillimeter megamaser activity, while for Circinus we confirm the results of Hagiwara et al. (2013), with an updated calibration. In both cases the 321 GHz spectra appear structurally comparable to those of the 22 GHz masers.

The continuum emission in NGC 5793 and NGC 4945 is well-resolved and spatially extended along the optical major axes of these galaxies, which are both edge-on spirals. This continuum is likely dominated by thermal emission from dust grains in the disk, and we use the observed fluxes to derive approximate ISM masses. For the other three galaxies, the continuum emission is centrally-concentrated and thus likely contains a substantial non-thermal component from the AGN.

Though the 22 GHz maser emission in Circinus is associated with both the accretion disk and a molecular outflow, it is unclear whether the 321 GHz emission traces both environments or just the disk. Furthermore, we have reason to believe that the 321 GHz masers trace the accretion disk at smaller radial separations from the central SMBH than the mapped 22 GHz masers do. This can be confirmed by future ALMA observations of Circinus, which should seek to obtain a map of the maser features at the highest possible angular resolution.

This paper makes use of the following ALMA data: 2011.0.00121.S. ALMA is a partnership of ESO (representing its member states), NSF (USA) and NINS (Japan), together with NRC (Canada) and NSC and ASIAA (Taiwan) and KASI (Republic of Korea), in co-operation with the Republic of Chile. The Joint ALMA Observatory is operated by ESO, AUI/NRAO and NAOJ. This research has made use of the NASA/IPAC Extragalactic Database (NED), which is operated by the Jet Propulsion Laboratory, California Institute of Technology, under contract with the National Aeronautics and Space Administration.

Facility: ALMA

Software: CASA

REFERENCES

- Braatz, J., Condon, J., Constantin, A., et al. 2015, IAU General Assembly, 22, #2255730
- Braatz, J. A., Wilson, A. S., & Henkel, C. 1996, ApJS, 106, 51
- Braatz, J. A., Wilson, A. S., Henkel, C., Gough, R., & Sinclair, M. 2003, ApJS, 146, 249
- Cernicharo, J., Pardo, J. R., & Weiss, A. 2006, ApJL, 646, L49
- Claussen, M. J., Heiligman, G. M., & Lo, K. Y. 1984, Nature, 310, 298
- Compiègne, M., Verstraete, L., Jones, A., et al. 2011, A&A, 525, A103
- Dos Santos, P. M., & Lepine, J. R. D. 1979, Nature, 278, 34
- Draine, B. T. 2003, ARA&A, 41, 241
- Elmouttie, M., Haynes, R. F., Jones, K. L., et al. 1997, MNRAS, 284, 830
- Fouque, P., Durand, N., Bottinelli, L., Gouguenheim, L., & Paturel, G. 1990, A&AS, 86, 473

- García-Burillo, S., Combes, F., Usero, A., et al. 2014, *A&A*, 567, A125
- Gardner, F. F., & Whiteoak, J. B. 1982, *MNRAS*, 201, 13P
- Gardner, F. F., Whiteoak, J. B., Norris, R. P., & Diamond, P. J. 1992, *MNRAS*, 258, 296
- Gray, M. D., Baudry, A., Richards, A. M. S., et al. 2016, *MNRAS*, 456, 374
- Greenhill, L. J., Ellingsen, S. P., Norris, R. P., et al. 1997a, *ApJL*, 474, L103
- Greenhill, L. J., Kondratko, P. T., Lovell, J. E. J., et al. 2003a, *ApJL*, 582, L11
- Greenhill, L. J., Moran, J. M., & Herrnstein, J. R. 1997b, *ApJL*, 481, L23
- Greenhill, L. J., Booth, R. S., Ellingsen, S. P., et al. 2003b, *ApJ*, 590, 162
- Hagiwara, Y., Kohno, K., Kawabe, R., & Nakai, N. 1997, *PASJ*, 49, 171
- Hagiwara, Y., Miyoshi, M., Doi, A., & Horiuchi, S. 2013, *ApJL*, 768, L38
- Henkel, C., Guesten, R., Downes, D., et al. 1984, *A&A*, 141, L1
- Henkel, C., Wouterloot, J. G. A., & Bally, J. 1986, *A&A*, 155, 193
- Humphreys, E. M. L., Greenhill, L. J., Reid, M. J., et al. 2005, *ApJL*, 634, L133
- Karachentsev, I. D., Makarov, D. I., & Kaisina, E. I. 2013, *AJ*, 145, 101
- Krips, M., Martín, S., Eckart, A., et al. 2011, *ApJ*, 736, 37
- Lo, K. Y. 2005, *ARA&A*, 43, 625
- Narayan, R. 1992, *Philosophical Transactions of the Royal Society of London Series A*, 341, 151
- Nasonova, O. G., de Freitas Pacheco, J. A., & Karachentsev, I. D. 2011, *A&A*, 532, A104
- Neufeld, D. A., & Melnick, G. J. 1991, *ApJ*, 368, 215
- Planck Collaboration, Abergel, A., Ade, P. A. R., et al. 2011, *A&A*, 536, A21
- . 2014, *A&A*, 571, A11
- Reid, M. J., & Honma, M. 2014, *ARA&A*, 52, 339
- Remijan, A., Adams, M., Akiyama, E., et al. 2015, *ALMA Cycle 3 Technical Handbook Version 1.0*
- Scoville, N., Aussel, H., Sheth, K., et al. 2014, *ApJ*, 783, 84
- Trotter, A. S., Greenhill, L. J., Moran, J. M., et al. 1998, *ApJ*, 495, 740
- Tully, R. B., Courtois, H. M., Dolphin, A. E., et al. 2013, *AJ*, 146, 86
- Vila Vilaro, B., Leon, S., Dent, W., et al. 2011, *ALMA Cycle 0 Technical Handbook Version 1.0*